Chapter 7
The Preparation and Applications of g-C$_3$N$_4$/TiO$_2$ Heterojunction Catalysts

7.1 Introduction

Nowadays, there have been two global problems all the society is facing, environmental pollution and energy shortage, which have caused great harm to human health and life. To solve these problems, photocatalysis as an effective approach has attracted widespread concern of researchers. In this approach, by utilizing photocatalysts, light as a clean excitation power can be used to induce a series of catalytic reactions, with regard to environment and energy, such as photocatalytic degradation of pollutants in water [1–4], removal of indoor harmful gases [5], reduction of CO$_2$ [6–8], as well as splitting of water to produce H$_2$ and O$_2$ [9].

In many of the photocatalysts studied, TiO$_2$ has been widely recognized as the most potential one due to its merits of low cost, good stability, nontoxicity, and so on [10–13]. However, the conventional TiO$_2$ has shortcomings in the following two aspects: (1) the large bandgap (~3.2 eV) can only absorb UV light with $\lambda \leq 387$ nm, and the absorption of visible light is almost zero, which leads to the low utilization efficiency of sunlight, and (2) the recombination rate of photo-generated electron–hole pairs is high, greatly limiting the photocatalytic performance of TiO$_2$. At present, various methods for the improvement of the photocatalytic activity of TiO$_2$ have been reported, such as metal and nonmetal oxide loading [14, 15], noble metal deposition [16, 17], nonmetal element doping [18, 19], modifications of morphology, and so on [20–23]. These methods can broaden the absorption wavelength of TiO$_2$ and enhance the absorption efficiency of solar light in some extent. But the recombination of photo-generated electrons and holes results in a lower quantum yield, further seriously affecting the catalytic activity of the catalysts.

Heterojunction catalyst is one of the hot spots in catalytic field in recent years, which usually consists of two different semiconductors contacting with each other to form the structure of heterojunction. The heterojunction structure can promote the transfer of the photo-generated electrons and holes in opposite direction, greatly improving the effective utilization rate of the excitons. Therefore, heterojunction

catalyst possesses better catalytic effect than that of single-component catalyst. Nowadays, there have been a great number of materials which can be used to modify TiO$_2$ by forming the heterojunction structure, such as ZnO [24, 25], SnO$_2$ [26, 27], g-C$_3$N$_4$, etc. [28–31]. Among them, g-C$_3$N$_4$ as a stable nonmetal semiconductor has attracted much attention in the catalytic field. Due to its special triazine structure, g-C$_3$N$_4$ exhibits many special properties including low density, high chemical stability, enhanced biological compatibility, good abrasion resistance, and so on. In addition, the relatively narrow bandgap of g-C$_3$N$_4$ (about 2.7 eV) extends its light response to visible region (about 450 nm). Zhang et al. reported that the g-C$_3$N$_4$ exhibited high photocatalytic performance for water splitting under visible light irradiation [32]. Dong and coworkers facilely synthesized polymeric g-C$_3$N$_4$-layered catalyst by directly heating urea or thiourea [33, 34]. In the research on heterojunction catalysts, g-C$_3$N$_4$ has gained the majority of researchers' attention owing to its simple preparation method, abundant kinds of precursors, as well as the advantages of low cost, becoming the first choice to form heterojunction with TiO$_2$.

In this chapter, the recent developments of the research on the heterojunction photocatalysts formed by g-C$_3$N$_4$ and TiO$_2$ were introduced, including its synthesis methods and applications. Firstly, the synthesis methods were summarized based on the synthesis order of each component during the preparation process and divided into three categories. In each category, the preparation procedures as well as their advantages and drawbacks were introduced in detail. Through these synthesis methods, an efficient heterojunction structure can be obtained between g-C$_3$N$_4$ and TiO$_2$. The photocatalytic activity of the photocatalysts can be greatly enhanced due to the formation of the heterojunction structure, which can effectively promote the separation of photo-generated charge carriers [35, 36]. The excellent photocatalytic activity of the g-C$_3$N$_4$/TiO$_2$ heterojunction photocatalysts enables them to be applied in many aspects. Therefore, the chapter also introduced the applications of g-C$_3$N$_4$/TiO$_2$ heterojunction photocatalysts in the field of photocatalysis, containing depollution of environment, hydrogen generation, photofixation of carbon dioxide, bacteria disinfection, and so on. In the end of the chapter, a short summary and outlook on the development of g-C$_3$N$_4$/TiO$_2$ heterojunction photocatalysts were provided.

7.2   The Preparation Methods of g-C$_3$N$_4$/TiO$_2$ Heterojunction Catalyst

Because the g-C$_3$N$_4$/TiO$_2$ heterojunction photocatalyst consists of two single-component g-C$_3$N$_4$ and TiO$_2$, the synthesis methods of g-C$_3$N$_4$/TiO$_2$ heterojunction catalyst can be classified into three categories according to the order of synthesis of each component: (1) physically mixing TiO$_2$ and g-C$_3$N$_4$, (2) growing g-C$_3$N$_4$ on TiO$_2$ catalyst, and (3) loading TiO$_2$ on g-C$_3$N$_4$ catalyst. No matter what the method

is, the final aim is to make g-C$_3$N$_4$ and TiO$_2$ contact with each other, further forming a heterojunction structure between g-C$_3$N$_4$ and TiO$_2$.

7.2.1   Physically Mixing g-C$_3$N$_4$ and TiO$_2$

This preparation method refers to firstly synthesizing g-C$_3$N$_4$ and TiO$_2$, respectively, and then physically mixing the two components together by ball milling or evaporation of dispersion solution. Hongjian Yan et al. prepared TiO$_2$-C$_3$N$_4$ by mixing TiO$_2$ and g-C$_3$N$_4$ powder using a ball milling method with different contents of g-C$_3$N$_4$. The TiO$_2$ was synthesized by the hydrolysis of TiCl$_4$ in ammonia, and the g-C$_3$N$_4$ was prepared by directly heating melamine at an atmosphere of Ar [37]. Yongfa Zhu et al. also fabricated g-C$_3$N$_4$/TiO$_2$ hybrid photocatalysts by a facile ball milling method. In their experiments, g-C$_3$N$_4$ was synthesized by directly heating melamine, and g-C$_3$N$_4$/TiO$_2$ photocatalysts were obtained by mixing g-C$_3$N$_4$ and TiO$_2$ powder in a ball mill. Their results showed that a layered structure of g-C$_3$N$_4$ was formed on the surface of TiO$_2$ [38]. Interestingly, they found that the as-prepared catalyst showed highly enhanced photocatalytic performance and the photocatalytic efficiency increased gradually with the increase of milling rate.

Apart from the ball milling, solvent evaporation is also a commonly used physical mixing method for the synthesis of g-C$_3$N$_4$/TiO$_2$ heterojunction photocatalyst. In this preparation process, g-C$_3$N$_4$ and TiO$_2$ are homogeneously dispersed in a solvent such as methanol, and then the solvent is evaporated to make g-C$_3$N$_4$ and TiO$_2$ contact with each other and thus form the heterojunction structure. Jingyu Wang et al. hybridized anatase TiO$_2$ nanosheets with dominant (001) facets with g-C$_3$N$_4$ via this facile solvent evaporation method. The polymeric g-C$_3$N$_4$ was synthesized by directly calcinating urea, and the anatase TiO$_2$ nanosheets with dominant (001) facets were prepared by a solvothermal reaction of tetrabutyl titanate (TBT). After the solvothermal treatment, the well-washed precipitate was dispersed into methanol and mixed with g-C$_3$N$_4$, followed by sonication for 30 min to completely disperse the g-C$_3$N$_4$. After that, the above sample was stirred in a fume hood for 12 h to evaporate the methanol, and the rest powder was dried at 100 °C for 4 h [39]. Dongjiang Yang et al. synthesized g-C$_3$N$_4$/TiO$_2$(B) nanofibers with exposed (001) plane with the enhanced visible light photoactivity through a facile solvent evaporation operation to the methanol solution of g-C$_3$N$_4$ and TiO$_2$ (B). The g-C$_3$N$_4$ was prepared by directly heating melamine in air at the temperature of 550 °C for 4 h, and TiO$_2$ (B) nanofibers were synthesized using a hydrothermal method combined with a subsequent calcination treatment [40]. Hong Huang et al. prepared heterostructured g-C$_3$N$_4$/Ag/TiO$_2$ microspheres with improved photocatalytic performance under visible light irradiation. As shown in Fig. 7.1, the protonated g-C$_3$N$_4$ sheets were synthesized by calcinating melamine and followed by the protonation in HCl solution, and TiO$_2$ nanomaterial was prepared by a typical hydrothermal method of Ti(OC$_4$H$_9$)$_4$, and then Ag/TiO$_2$ microspheres were obtained by depositing
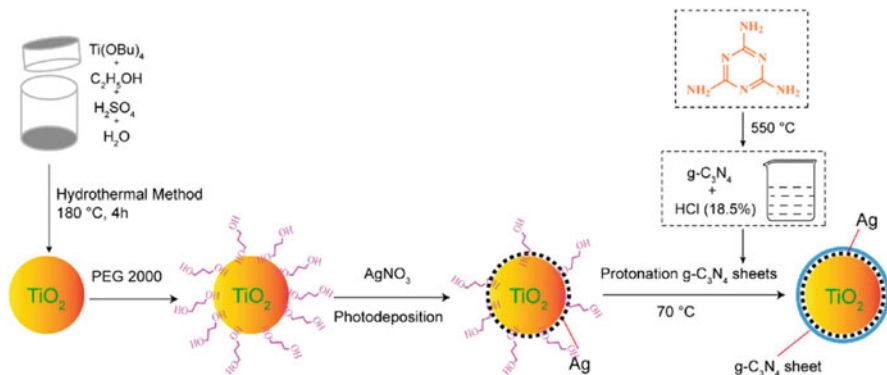
Fig. 7.1   Scheme for the synthesis of g-C$_3$N$_4$/Ag/TiO$_2$ microspheres [41] (Reprinted with permission from Ref. [41]. Copyright 2014, American Chemical Society)

Ag on the surface of TiO$_2$ microspheres, which was then mixed with g-C$_3$N$_4$ by forming suspension at 70 °C [41].

Guangshe Li et al. reported an effective visible light-driven photocatalyst of brookite TiO$_2$ (br-TiO$_2$) hybridized with g-C$_3$N$_4$ for the first time via a facile calcination of br-TiO$_2$ and g-C$_3$N$_4$ in air. The optimum photocatalytic activity of the as-prepared samples was higher than that of other phase types of TiO$_2$ (anatase and rutile) hybridized with g-C$_3$N$_4$ [42]. Tianyou Peng et al. synthesized porous g-C$_3$N$_4$ by a simple pyrolysis of urea, and Pt-TiO$_2$ was fabricated by photodepositing Pt on the TiO$_2$. Then g-C$_3$N$_4$–Pt-TiO$_2$ nanocomposite was synthesized via a facile chemical adsorption followed by a calcination treatment [30].

The physical mixing method for preparing g-C$_3$N$_4$/TiO$_2$ heterojunction catalyst is easy to operate and beneficial for scale-up, which provides a potential for mass production. However, uniform mixing may not be easy to achieve. In the aspect of designing catalyst, morphology control is widely considered as an effective way to improve the catalytic activity, while physical mixing method is difficult to achieve this goal. Moreover, the close contact between g-C$_3$N$_4$ and TiO$_2$ may be not easy to form, causing the poor stability of the heterojunction catalysts.

7.2.2   Growing TiO$_2$ on g-C$_3$N$_4$

In this method, g-C$_3$N$_4$ is firstly synthesized by one-step calcinations of precursors, and then the prepared g-C$_3$N$_4$ reacts with the precursor of TiO$_2$ to achieve the in situ growth of TiO$_2$ on the surface of g-C$_3$N$_4$. For example, Deliang Cui et al. fabricated g-C$_3$N$_4$/TiO$_2$ composite through this method. The g-C$_3$N$_4$ was synthesized by polymerization of dicyandiamide at the temperature of 600 °C for 5 h under N$_2$ atmosphere. Then the as-synthesized g-C$_3$N$_4$ was taken into the hydrolysis of Ti(OC$_4$H$_9$n)$_4$. After hydrothermal reaction, the hybrid composite of g-C$_3$N$_4$/TiO$_2$ was

obtained, which showed better photocatalytic activity than hybrid composite of g-C$_3$N$_4$/TiO$_2$ and the pure TiO$_2$ for degradation of rhodamine B (RhB) under the UV and visible light irradiation [28]. Similarly, Hongtao Yu et al. prepared g-C$_3$N$_4$/ TiO$_2$ hybrid photocatalyst with wide absorption wavelength range from 300 nm to 450 nm by taking g-C$_3$N$_4$ into the hydrolysis reaction of TiCl$_4$. TEM images showed that TiO$_2$ nanoparticles were dispersed well on the surface of g-C$_3$N$_4$ sheet, and the average size of particles was much smaller than that of TiO$_2$ samples without g-C$_3$N$_4$ sheet. The synthesized g-C$_3$N$_4$/TiO$_2$ exhibited much better photocatalytic activity for the degradation of phenol than pristine g-C$_3$N$_4$ and TiO$_2$ [43]. Qianhong Shen et al. developed a novel and facile template-free method to synthesize a network structure of mesoporous g-C$_3$N$_4$/TiO$_2$ nanocomposite with enhanced visible light photocatalytic activity. Firstly, they synthesized g-C$_3$N$_4$ by directly heating melamine, and then g-C$_3$N$_4$/TiO$_2$ was obtained by adding g-C$_3$N$_4$ into the solution of titanium sulfate Ti(SO$_4$)$_2$ and followed by hydrothermal reaction [44].

In recent years, more and more attention has been paid in the research on nitrogen-doped titanium dioxide (N-TiO$_2$), due to its promising extension for environmental application [2, 45]. Many groups grew the N-TiO$_2$ on the surface of g-C$_3$N$_4$ to form heterojunction. Fatang Li et al. reported an in situ microwave-assisted synthesis method to fabricate N-TiO$_2$/g-C$_3$N$_4$ composites by using H$_2$TiO$_3$ as the reactant and NH$_3$·H$_2$O as the N-doping source. In their experiments, they firstly took g-C$_3$N$_4$ into the H$_2$TiO$_3$ solution then followed by a microwave-assisted reaction. The preparation process was as shown in Fig. 7.2. The catalyst had a porous structure and large surface area, which increased the contact area of the catalyst with pollutants. The photocatalytic degradation of rhodamine B (RhB) and methylene blue (MB) with the as-prepared samples was carried out under visible light irradiation to evaluate the photocatalytic activity. Among them, N-TiO$_2$/g-C$_3$N$_4$ composite with 40 wt % of N-TiO$_2$ showed the highest photocatalytic activity [46].

Through heating the mixture of the hydrolysis product of TiCl$_4$ and g-C$_3$N$_4$ at different weight ratios, W. F. Zhang et al. successfully prepared N-doped TiO$_2$/C$_3$N$_4$ composite samples. Due to the introduction of g-C$_3$N$_4$, the composite samples showed slight visible light absorption. XPS result revealed that some nitrogen was doped into TiO$_2$, and g-C$_3$N$_4$ existed in the composite sample [29]. Similarly, as shown in Fig. 7.3, g-C$_3$N$_4$ nanosheets (g-C$_3$N$_4$ NSs) hybridized nitrogen-doped TiO$_2$ (N-TiO$_2$) nanofibers (GCN/NT NFs) have been synthesized in situ through a
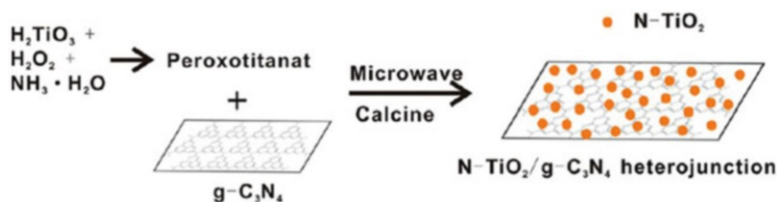

Fig. 7.2 Diagrammatic sketch for the in situ deposition of N-TiO$_2$ nanoparticles on g-C$_3$N$_4$ sheets [46]. (Reprinted with permission from Ref. [46]. Copyright 2013, American Chemical Society)
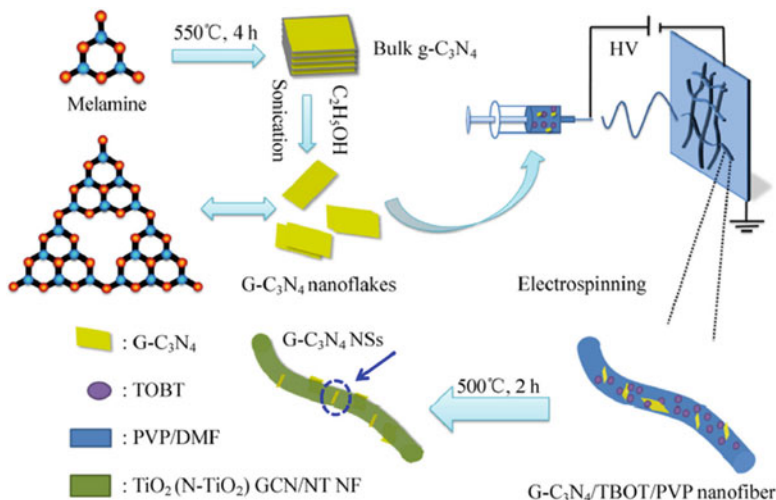
Fig. 7.3 Schematic illustration of the fabrication of GCN/NT NFs [47]. (Reprinted with permission from Ref. [47]. Copyright 2013, Springer)

simple electrospinning process combined with a modified heat-etching method by Cheng Han et al. [47]. The melamine was thermal polymerized to form g-C$_3$N$_4$, which was dispersed into acetic acid solution including poly(vinylpyrrolidone) (PVP) and titanium (IV) n-butoxide (TNBT). Doping nitrogen into TiO$_2$ narrowed its energy bandgap, and the catalyst could be activated under visible irradiations, leading to higher photocatalytic efficiency.

In addition, most of TiO$_2$ nanoparticles grown on the surface of g-C$_3$N$_4$ were present as crystals. Solvothermal reaction can control the exposure of high-energy surfaces. For example, Kangle Lv et al. grew TiO$_2$ hollow nanobox (TiO$_2$-HNB) assembled from high-energy TiO$_2$ nanosheets (TiO$_2$-NS) on g-C$_3$N$_4$ to form the g-C$_3$N$_4$/TiO$_2$ hybrid and investigated the effect of contact interfaces of high-energy TiO$_2$, (101) and (001) facets on the photocatalytic activity. The catalyst was fabricated through a solvothermal strategy using TBA as the solvent [48]. In our previous work, well-dispersed TiO$_2$ nanocrystals with (001) facets were successfully grown in situ on g-C$_3$N$_4$ through a facial solvothermal method, as shown in Fig. 7.4. During the solvothermal process, the ammonium acetate (AMAT) serving as a catalyst for the hydrolysis of tetrabutyl titanate (TBOT) was added into the nonaqueous system. In addition, because carboxylic acid is easy to adsorb on the surface of anatase (001), part of the acetic acid produced by the decomposition of AMAT serves as face-growth inhibitors, slowing the growth of the (001) facet of TiO$_2$ in the TiO$_2$ nanoparticles, leading to the exposure of high-energy facets. The characterization results showed an enhanced separation efficiency of photo-generated charge carriers compared with that of pure g-C$_3$N$_4$, and well-matched energy levels between TiO$_2$ and g-C$_3$N$_4$ altogether led to the enhancement of photocatalytic activity [49].
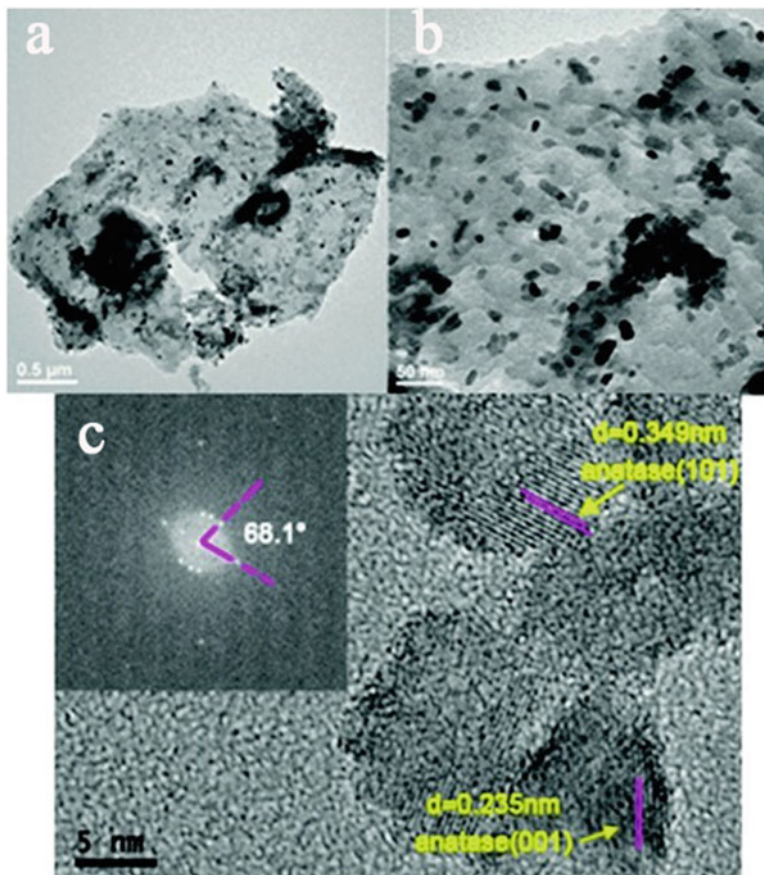
Fig. 7.4 (**a** and **b**) TEM images of TiO$_2$/g-C$_3$N$_4$(1.5) catalyst, (**c**) HRTEM image of TiO$_2$/g-C$_3$N$_4$(1.5) catalyst. Inset: the corresponding fast Fourier transform (FFT) pattern [49]. (Reprinted with permission from Ref. [49]. Copyright 2015, Royal Society of Chemistry)

The strategy of growing TiO$_2$ on g-C$_3$N$_4$ is very effective to form the heterojunction structure. The heterojunction which formed in the growing process possesses chemical stability during the multiple cycle experiments. However, due to the rapid hydrolysis process of the titanium precursor, it is difficult to achieve ultradispersed TiO$_2$ nanocrystals on the surface of g-C$_3$N$_4$ by this method [50]. Besides, a great challenge for controlling the microstructures of coupled TiO$_2$ with desired size distribution and dispersity still retains.

7.2.3 Loading g-C₃N₄ on TiO₂

In this synthesis method, TiO_2 is firstly obtained by hydrolysis, hydrothermal, microwave method, or directly using the commercial P25, and then TiO_2 is impregnated in the precursor solution of g-C_3N_4 to obtain the g-C_3N_4/TiO_2 heterojunction catalyst after drying and calcination. Weide Zhang et al. modified TiO_2 nanorod arrays with g-C_3N_4 via chemical vapor deposition using melamine as a precursor. The rutile TiO_2 nanorod arrays were firstly synthesized by hydrothermal process, and then the TiO_2/FTO was loaded with melamine and followed by heating process in a muffle furnace to obtain g-C_3N_4/TiO_2/FTO. The g-C_3N_4/TiO_2/FTO electrode exhibited high photoelectrocatalytic activity for degradation of RhB. Under visible light irradiation, the photocurrent response of the g-C_3N_4/TiO_2/FTO electrode is about 10 times as that of the TiO_2/FTO electrode, making it a promising nanomaterial for future applications in solar cells, water treatment, as well as photoelectric devices [51]. Min Fu et al. prepared a kind of novel visible light photocatalyst g-C_3N_4/TiO_2 composite by calcinating the mixtures of melamine and commercial TiO_2 at different weight ratios. In their work, the samples at the optimized precursor weight ratio ($M_{melamine}$: $M_{titania}$ = 2.5) exhibited highest adsorption ability and visible light photocatalytic activity, evaluated by photocatalytic degradation of methylene blue (MB) [52]. Furthermore, Min Fu et al. also synthesized novel g-C_3N_4-coated TiO_2 nanocomposites by a facile and cost-effective solid-state method through thermal treatment of the mixture of urea and commercial TiO_2. The as-prepared g-C_3N_4-coated TiO_2 nanocomposites showed efficient visible light photocatalytic activity for degradation of aqueous MB owing to the increased visible light absorption and enhanced MB adsorption [31]. Burapat Inceesungvorn et al. fabricated g-C_3N_4/TiO_2 films by directly heating the mixture of melamine and pre-synthesized TiO_2 nanoparticles at the atmosphere of Ar. The TiO_2 was prepared by hydrolysis of titanium tetraisopropoxide (TTIP) and calcination. The obtained samples showed enhanced photocatalytic degradation of MB. In addition, as Fig. 7.5

Fig. 7.5 MB photolysis and photocatalytic degradation using pure TiO_2, pure g-C_3N_4, and g-C_3N_4/TiO_2 composite films as photocatalysts [53]. (Reprinted with permission from Ref. [53]. Copyright 2014, Elsevier)
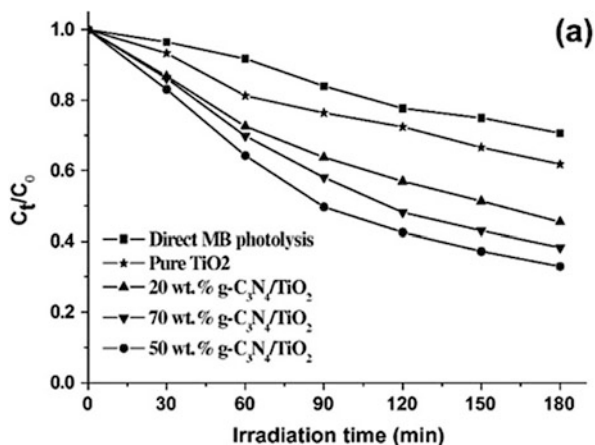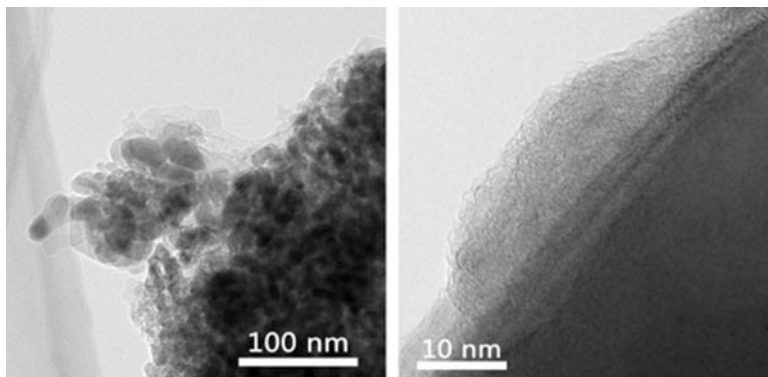
Fig. 7.6 TEM image of g-C$_3$N$_4$-modified TiO$_2$ composites [55]. (Reprinted with permission from Ref. [55]. Copyright 2015, Elsevier)

shows, the 50 wt% g-C$_3$N$_4$/TiO$_2$ composite with the best loading content exhibited the best performance [53].

Honglei Zhu et al. synthesized a series of g-C$_3$N$_4$-P25 composite photocatalysts with different mass ratios using an in situ preparation method. In the method, g-C$_3$N$_4$-P25 nanocomposites were obtained by calcinating mixtures of the P25 and dicyandiamide. The optimal g-C$_3$N$_4$ content was determined to be 84%. The sample in the optimal weight ratio exhibited almost 3.3 times higher photocatalytic activity than that of individual g-C$_3$N$_4$ under visible light irradiation [54]. Our group also prepared g-C$_3$N$_4$-modified TiO$_2$ composites through a simple calcination process of anatase and cyanamide. TEM images of as-synthesized catalyst, presented in Fig. 7.6, show TiO$_2$ is covered by a thin shell of g-C$_3$N$_4$, and the polymer shell on the surface is around 5–10 nm thick. The photocatalytic activities of the composites were evaluated by photocatalytic degradation of Acid Orange 7 (AO7). The photocatalyst showed excellent activity under both visible and UV light. In addition, no nitrogen doping was found in TiO$_2$ lattice, demonstrating the g-C$_3$N$_4$ was surface attached on TiO$_2$ and ascribing all improvement of photocatalytic activity of g-C$_3$N$_4$/ TiO$_2$ composite to the synergy between TiO$_2$ and g-C$_3$N$_4$ [55]. After that, we reported a highly condensed g-C$_3$N$_4$-modified TiO$_2$ photocatalyst prepared by a vacuum calcination method. A close-to-theoretical C/N ratio was detected in the catalyst by element analysis. The results indicated a complete and neat polymerization of the g-C$_3$N$_4$ on TiO$_2$. Excellent photocatalytic activities of as-prepared catalysts have been achieved under both visible and UV light irradiation. The heterojunction can be easily obtained during the calcination process, and the preparation procedures are easy to operate, but the amount of loading g-C$_3$N$_4$ is influenced by numerous factors, such as gas condition, flow rate, heating temperature, and heating rate [56].

Photochemical and electrochemical methods were also developed to load g-C$_3$N$_4$ on TiO$_2$. These methods are hard to control, but this in situ growth strategy has drawn more and more attention in recent years. Xiaoxin Zou et al. synthesized

mesoporous TiO$_2$ spheres with a large surface area and rich surface hydroxyl groups by a light-driven synthetic strategy. It can be used for activating urea under a mild condition to form g-C$_3$N$_4$ material [57]. Xiaosong Zhou et al. synthesized a g-C$_3$N$_4$/TiO$_2$ nanotube array (CN/TNT) heterojunction photocatalyst with visible light response via a simple electrochemical method. g-C$_3$N$_4$ polymer was deposited into the crystallized TiO$_2$ nanotubes by electrodeposition [58].

In this method, because TiO$_2$ is prepared firstly, it is allowed for selection or structure design of TiO$_2$, but the high-temperature calcination for the formation of g-C$_3$N$_4$ is prone to resulting in the aggregation of TiO$_2$ and may lead to a negative impact on the improvement of photocatalytic activity.

7.3   The Applications of g-C$_3$N$_4$/TiO$_2$ Heterojunction Catalyst

Compared with single-component catalysts, the g-C$_3$N$_4$/TiO$_2$ heterojunction catalysts formed by the combination of g-C$_3$N$_4$ and TiO$_2$ show greatly enhanced photocatalytic activity. Therefore, fabricating the g-C$_3$N$_4$/TiO$_2$ has many promising applications in various fields of photocatalysis. Currently, the researches on the applications of g-C$_3$N$_4$/TiO$_2$ mainly focus on the degradation of organic pollutants, hydrogen generation from water, photocatalytic reduction of CO$_2$, treatment of heavy metal ion, and inactivation of bacteria.

7.3.1   Degradation of Organic Pollutants

With the rapid development of economy, environmental pollution problems have greatly affected our daily lives, among which the most serious problems are water pollution and air pollution. The majority in the source of pollution is organic pollutants. Therefore, the degradation of organic pollutants is a hot research topic in recent decades. Various kinds of g-C$_3$N$_4$/TiO$_2$ heterojunction catalysts have also been developed and applied to solve these pollution problems.

7.3.1.1   Degradation of Pollutants in Liquid Phase

Many research works have been carried out to examine the photocatalytic degradation of organic dyes such as RhB and AO7 in aqueous solution in the presence of g-C$_3$N$_4$/TiO$_2$ heterojunction catalyst. For instance, methyl blue (MB) was degraded by g-C$_3$N$_4$/TiO$_2$ catalyst which was synthesized by directly heating the mixture of urea and commercial TiO$_2$ [31]. The catalyst exhibited efficient photocatalytic degradation of MB under visible light irradiation. The degradation efficiency can
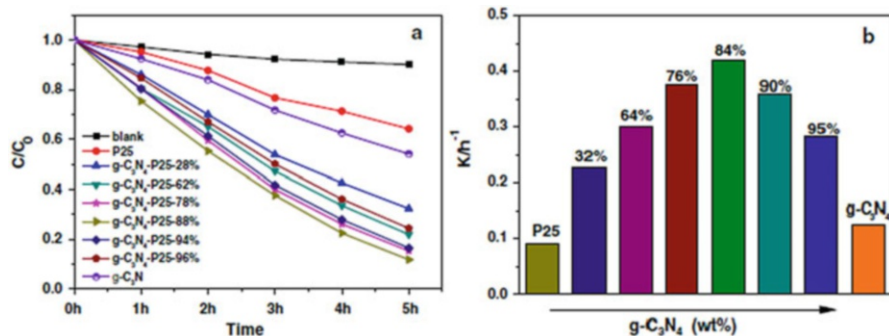
Fig. 7.7 (**a**) Photolysis and photocatalytic degradation of MB with TiO$_2$, g-C$_3$N$_4$, and g-C$_3$N$_4$-P25 photocatalysts. (**b**) Degradation rate constants of MB over TiO$_2$, g-C$_3$N$_4$, and g-C$_3$N$_4$-P25 photocatalysts [54]. (Reprinted with permission from Ref. [54]. Copyright 2015, Springer)

be adjusted by tuning the treatment temperature in the synthesis process of the composite catalyst, and the g-C$_3$N$_4$/TiO$_2$ nanocomposite prepared at 450 °C exhibited the best photocatalytic performance, which was much higher than the pure TiO$_2$. In addition to the preparation temperature, the mass ratio between g-C$_3$N$_4$ and TiO$_2$ also had a great influence on the degradation efficiency. Honglei Zhu et al. fabricated g-C$_3$N$_4$-P25 composite catalysts with different mass ratios and examined their photocatalytic activity toward the degradation of MB [54]. As shown in Fig. 7.7, the degradation efficiency varied with different g-C$_3$N$_4$ and P25 mass ratios. The sample with an optimal g-C$_3$N$_4$ content of 88% exhibited the highest photocatalytic activity which was almost 3.3 times higher than that of pure g-C$_3$N$_4$ under visible light irradiation.

In addition to MB, other dyes were also degraded by the g-C$_3$N$_4$/TiO$_2$ heterojunction photocatalysts. Photocatalytic degradation of RhB and MB was carried out by Fatang Li et al. to test the visible light photocatalytic activity of N-TiO$_2$/g-C$_3$N$_4$. As Fig. 7.8 shows, N-TiO$_2$/g-C$_3$N$_4$ composite with 40 wt% of N-TiO$_2$ showed the highest photocatalytic activity. The efficient separation of photo-generated electrons and holes, which resulted from the formation of N-TiO$_2$/g-C$_3$N$_4$ heterostructure, led to the excellent photocatalytic performance [46]. Guohong Wang et al. also degraded RhB using a novel macro-/mesoporous g-C$_3$N$_4$/TiO$_2$ heterojunction photocatalyst. The good photocatalytic activity of this kind of product ascribed to the fact that the sample possessed a large specific surface area and an excellent heterostructure [59]. Xiaosong Zhou et al. synthesized a carbon nitride/TiO$_2$ nanotube array (CN/TNT), and the catalyst exhibited high photocatalytic activity toward the degradation of methyl orange (MO) [58]. They prepared the photocatalysts denoted as CT$_x$ (x represents the deposition time) by electrodeposition of g-C$_3$N$_4$ into the crystallized TiO$_2$ nanotubes. Their experimental results showed that the photocatalytic activities of CN/TNTs increased as the deposition time increased at the first, then decreased, and the CT$_{5.0}$ exhibited the highest photocatalytic activity.
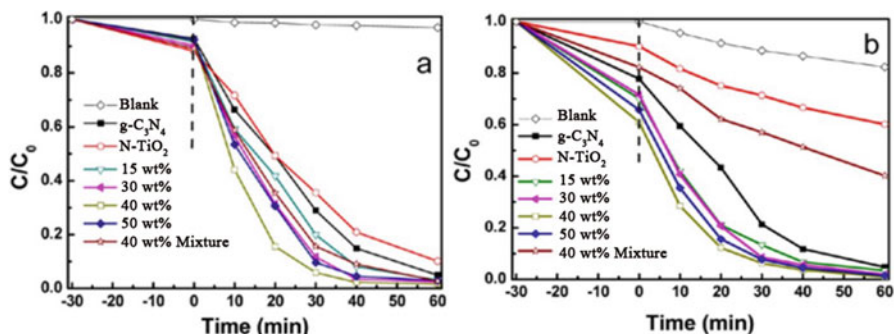
Fig. 7.8 Photocatalytic activities of N-TiO$_2$, g-C$_3$N$_4$, and N-TiO$_2$/g-C$_3$N$_4$ composites on the photodegradation of (**a**) RhB and (**b**) MB driven by visible light irradiation [46]. (Reprinted with permission from Ref. [46]. Copyright 2013, American Chemical Society)
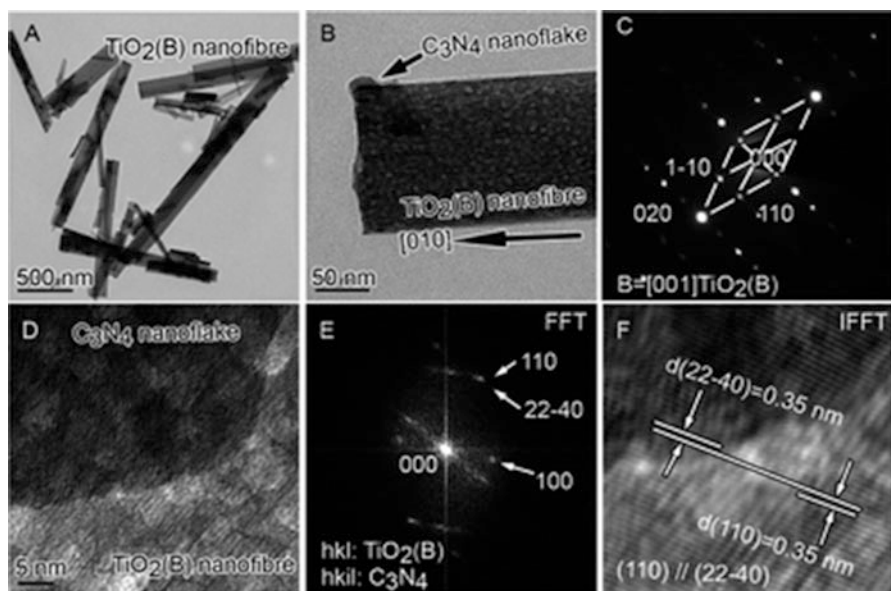

Fig. 7.9 (**a** and **b**) TEM images of the g-C$_3$N$_4$/TiO$_2$(B)-1 catalyst; (**c**) EDP of the g-C$_3$N$_4$/TiO$_2$(B)-1 catalyst; (**d**) HRTEM image of a g-C$_3$N$_4$ nanoflake deposited on the TiO$_2$(B) nanofiber; (**e**) fast Fourier transformation (FFT) image of the joint area between TiO$_2$(B) and g-C$_3$N$_4$ in image; (D), (**f**) inverse fast Fourier transformation (IFFT) image of g-C$_3$N$_4$/TiO$_2$(B)-1 sample [40]. (Reprinted with permission from Ref. [40]. Copyright 2014, Royal Society of Chemistry)

Dongjiang Yang et al. synthesized g-C$_3$N$_4$/TiO$_2$(B) nanofibers with selective exposure of high-energy (001) plane and applied it to the degradation of sulforhodamine B (SRB) dye. Figure 7.9 revealed that the diffraction spots of electron diffraction pattern (EDP) of samples could be indexed as (110), (1–10),
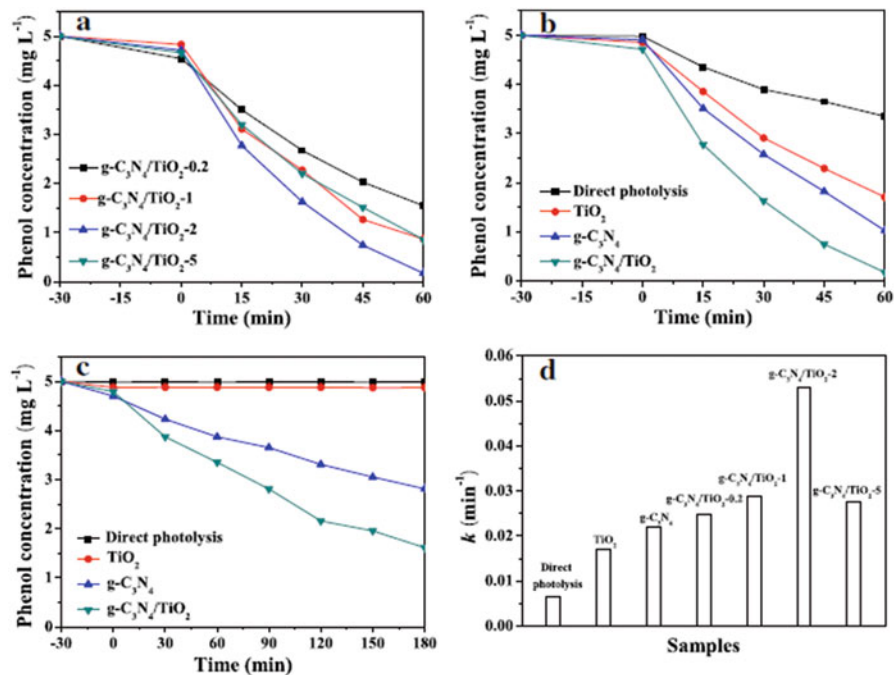
Fig. 7.10 (**a**) Photocatalytic degradation of phenol using g-C$_3$N$_4$/TiO$_2$ catalysts with various weight ratios under full-spectrum irradiation; (**b**) photocatalytic degradation of phenol by g-C$_3$N$_4$, TiO$_2$, and g-C$_3$N$_4$/TiO$_2$ under full-spectrum irradiation and (**c**) under visible light irradiation; (**d**) the kinetic constants of phenol degradation under full-spectrum irradiation [43]. (Reprinted with permission from Ref. [43]. Copyright 2012, Elsevier)

and (020). The g-C$_3$N$_4$/TiO$_2$(B) system showed better photocatalytic degradation ability than the g-C$_3$N$_4$/anatase system, although the photocatalytic activity of the anatase nanofibers was much better than that of the TiO$_2$(B) nanofibers [40].

In addition to dyes, some other organic compounds such as phenol have also been served as the target pollutants in the g-C$_3$N$_4$/TiO$_2$ photocatalysis system. For example, Hongtao Yu et al. investigated the photocatalytic activity of g-C$_3$N$_4$/TiO$_2$ for the photocatalytic degradation of phenol under visible and UV light. The g-C$_3$N$_4$/TiO$_2$ exhibited higher photocatalytic activity than pure TiO$_2$ and g-C$_3$N$_4$, as shown in Fig. 7.10, and the g-C$_3$N$_4$/TiO$_2$–2 with the mass ratio of g-C$_3$N$_4$/TiO$_2$ = 2 possessed the best photocatalytic activity [43].

In addition, a kind of TiO$_2$/g-C$_3$N$_4$ catalyst with highly dispersed TiO$_2$ nanocrystals on g-C$_3$N$_4$ has also been used for the photocatalytic degradation of phenol by Jinlong Zhang et al. It was found that high dispersion of TiO$_2$ with high-energy (001) facet was beneficial for the enhancement of the photocatalytic activity. As Fig. 7.11a shows, the photocatalytic activity of TiO$_2$/g-C$_3$N$_4$ catalysts showed an obvious increase for phenol decomposition compared with the pure TiO$_2$ and g-C$_3$N$_4$. The optimal catalyst TiO$_2$/g-C$_3$N$_4$(1.5) successfully degraded 100% phenol
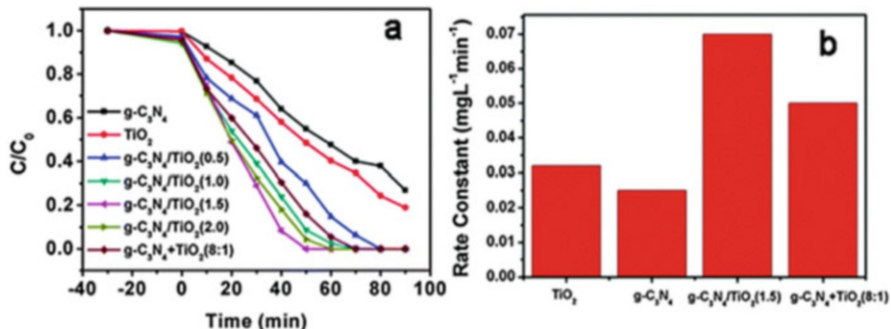
Fig. 7.11 Photocatalytic degradation results of 10 mg L^{-1}phenol with different catalysts under simulated sunlight irradiation of 300 W xenon lamp coupled with AM 1.5 [49]. (Reprinted with permission from Ref. [49]. Copyright 2015, Royal Society of Chemistry)
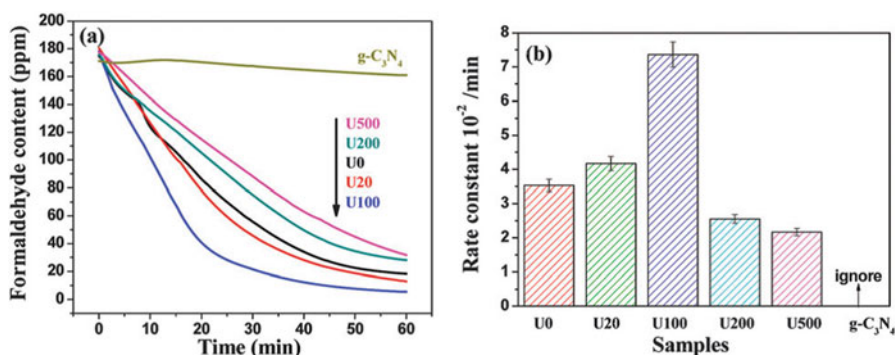

Fig. 7.12 The photocatalytic decomposition results of HCHO in air using U0, U20, U100, U200, U500, and g-C$_3$N$_4$ samples, respectively. (**a**) The corresponding concentration–time plots of HCHO; (**b**) the decomposition rate constant for all samples [5]. (Reprinted with permission from Ref. [5]. Copyright 2013, Royal Society of Chemistry)

within 50 min, whose rate constant was about 2.2 times that of pure TiO$_2$ and 2.8 times that of pure g-C$_3$N$_4$ (Fig. 7.11b) [49].

7.3.1.2 Degradation of Pollutants in Gas Phase

The status of air quality has great influence on people's health. After interior decoration, the concentration of formaldehyde (HCHO) in the air will rise sharply, causing a great impair to people's health. Jiaguo Yu et al. synthesized g-C$_3$N$_4$-TiO$_2$ photocatalyst and applied it for the photocatalytic oxidation decomposition of HCHO in air. As shown in Fig. 7.12, the weight percentage ratio of urea against P25 in the precursors was tuned to be 0, 20, 100, 200, and 500 (wt%), and the resulting catalysts were labeled as Ux (x represented the urea to P25 weight ratio),
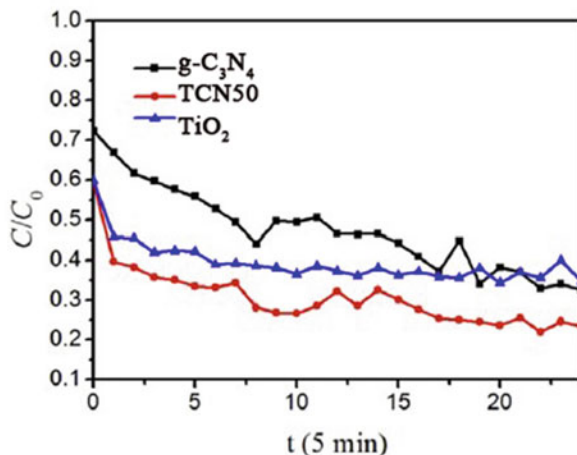
Fig. 7.13 Photocatalytic degradation results of gaseous acetone under the simulated solar light irradiation [60]. (Reprinted with permission from Ref. [60]. Copyright 2016, Elsevier)

and its value was equal to 0, 20, 100, 200, and 500, respectively. Their experimental results showed that the pure g-C$_3$N$_4$ exhibited very low photocatalytic activity for HCHO oxidation decomposition, while pure TiO$_2$ was active for decomposition of HCHO, and the photocatalytic activity of g-C$_3$N$_4$-TiO$_2$ was highly dependent on the amount of incorporated g-C$_3$N$_4$. The U100 sample with g-C$_3$N$_4$ content of 94% exhibited the highest photocatalytic activity for HCHO decomposition [5].

In addition to formaldehyde, gaseous acetone has also been degraded by the g-C$_3$N$_4$/TiO$_2$ photocatalyst. Xiangli Li fabricated microspherical g-C$_3$N$_4$/TiO$_2$ with high percentage of TiO$_2$ (001) facets through a solvothermal method and evaluated its photocatalytic activity for the degradation of gaseous acetone [60]. As Fig. 7.13 shows, the g-C$_3$N$_4$/TiO$_2$ catalyst (TCN50) could degrade more than 70% acetone within 120 min under simulated solar light irradiation. The photocatalytic efficiency of g-C$_3$N$_4$/TiO$_2$ for degrading acetone was much higher than that of pure g-C$_3$N$_4$ and TiO$_2$. Moreover, their experimental results also proved that acetone was oxidized by the highly active O$_2$· into CO$_2$ and H$_2$O in their reaction system.

In the process of the degradation of the gaseous pollutants, the adsorption capacity of the catalyst was the main factor, which greatly affects the photocatalytic activity. Tailoring the performance of materials via adjusting the morphologies and structures of the catalysts has emerged as a new and important direction of the research on g-C$_3$N$_4$/TiO$_2$ heterojunction catalyst for the photocatalytic degradation of gaseous organic pollutants.

7.3.2 Hydrogen Generation from Water

Due to the fact of the global energy depletion, the development and production of new sources of energy especially the clean energy have attracted more and more experimental interests. Hydrogen is widely considered as a highly effective

Fig. 7.14 The average hydrogen production rates as a function of wt% of g-C$_3$N$_4$ in the TiO$_2$-g-C$_3$N$_4$ composite from the first 3 h of the reaction duration [37]. (Reprinted with permission from Ref. [37]. Copyright 2011, Elsevier)
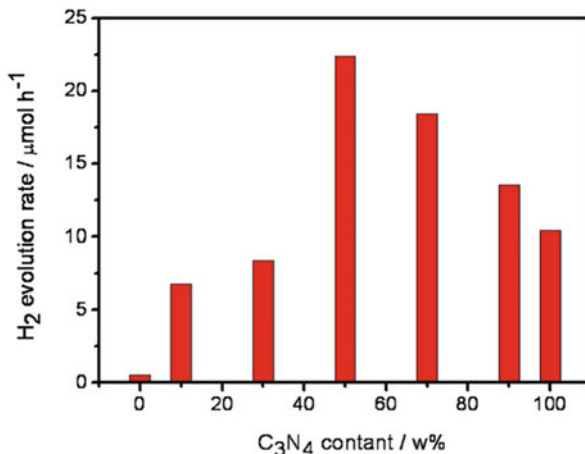
environmental and green energy, whose production methods have been studied and explored a lot. Among the numerous production methods, water splitting with g-C$_3$N$_4$/TiO$_2$ as photocatalyst has been favored by many researchers due to its merit of environment friendly.

Hongjian Yan et al. fabricated TiO$_2$-g-C$_3$N$_4$ composite catalysts with varying the wt% of g-C$_3$N$_4$ and used the samples in photocatalytic H$_2$ generation. The visible light-induced H$_2$ evolution rate was remarkably improved by coupling TiO$_2$ with g-C$_3$N$_4$, and the sample TiO$_2$–50 wt% C$_3$N$_4$ showed the highest activity, as shown in Fig. 7.14 [37].

Tianyou Peng et al. prepared porous g-C$_3$N$_4$-Pt-TiO$_2$, and their experimental results showed that coupling TiO$_2$ with g-C$_3$N$_4$ could remarkably enhance the visible light-induced photocatalytic hydrogen evolution rate. Besides, the g-C$_3$N$_4$-Pt-TiO$_2$ composite with a mass ratio of 70:30 exhibited the maximum photocatalytic activity as well as excellent photostability for hydrogen production under visible light irradiation (Fig. 7.15) [30].

Zhenyi Zhang et al. synthesized ternary heterostructured nanofibers (NFs) consisting of g-C$_3$N$_4$ nanosheets (NSs), plasmonic noble metal nanoparticles (Au, Ag, or Pt NPs), and TiO$_2$ NPs. The ternary composite photocatalyst exhibited improved charge-carrier migration efficiency and achieved highly efficient photocatalytic H$_2$ evolution [61]. Yanping Hong et al. prepared an anatase boron-doped TiO$_2$ (B-TiO$_2$) with exposed (001) facets and composited it with the g-C$_3$N$_4$ to form B-TiO$_2$–001/g-C$_3$N$_4$ heterojunctions. The heterojunction photocatalyst had the greatest photocatalytic activity for H$_2$ production as shown in Fig. 7.16, which was ascribed to the broad range of visible light absorption, the efficiently reduced charge recombination, and relatively higher catalytic activity of (001) facets compared to the (101) facets [62].

In addition, Yan-Yan Song et al. modified the g-C$_3$N$_4$/TiO$_2$ nanotube arrays with Pt nanoparticles. Compared with g-C$_3$N$_4$-free aligned TiO$_2$ nanotube layers, the obtained sample exhibited a strong enhancement for photoelectron–chemical and
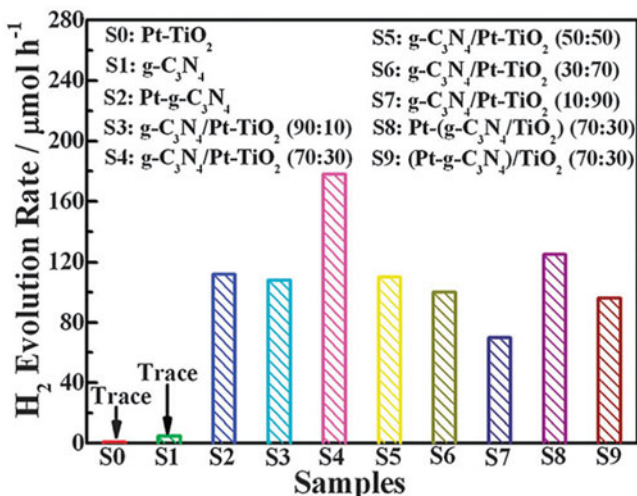
Fig. 7.15 Photocatalytic H$_2$ evolution rates of Pt-TiO$_2$, g-C$_3$N$_4$, Pt-g-C$_3$N$_4$, and g-C$_3$N$_4$–Pt-TiO$_2$ composites in different mass ratios as well as Pt-(g-C$_3$N$_4$–TiO$_2$) and (Pt-g-C$_3$N$_4$)/TiO$_2$ composites with a mass ratio of 70:30 under visible light irradiation [30]. (Reprinted with permission from Ref. [30]. Copyright 2012, Royal Society of Chemistry)

Fig. 7.16 Photocatalytic H$_2$ evolution of the as-synthesized samples: (*a*) g-C$_3$N$_4$, (*b*) TiO$_2$–001, (*c*) B-TiO$_2$–001, (*d*) TiO$_2$–001/ g-C$_3$N$_4$ (5.0%), (*e*) P25/g-C$_3$N$_4$ (5.0%), (*f*) B-TiO$_2$–001/g-C$_3$N$_4$ (1.0%), (*g*) B-TiO$_2$–001/g-C$_3$N$_4$ (2.0%), (*h*) B-TiO$_2$–001/g-C$_3$N$_4$ (5.0%), (*i*) B-TiO$_2$–001/g-C$_3$N$_4$ (10%) [62]. (Reprinted with permission from Ref. [62]. Copyright 2016, Elsevier)
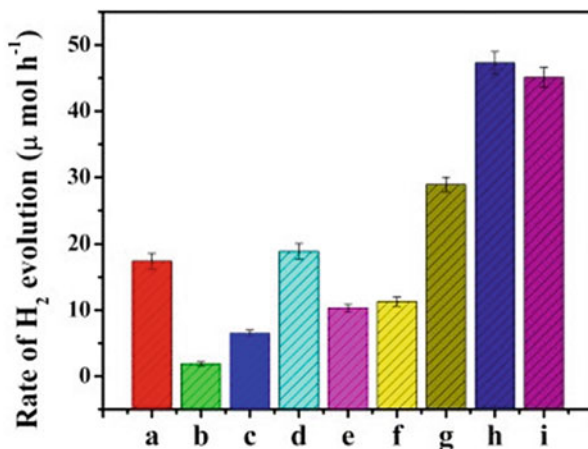
bias-free H$_2$ evolution of 15.62 μL h^{-1} cm^{-2}, which was almost a 98-fold increase in the H$_2$ production rate of aligned TiO$_2$ nanotube layers (0.16 μL h^{-1} cm^{-2}) [63]. Jian-guo Wang et al. designed and fabricated a novel g-C$_3$N$_4$/TiO$_2$ nanobelt heterostructure material. As shown in Fig. 7.17, the g-C$_3$N$_4$/TiO$_2$ nanobelt heterostructure with a mass ratio of 3:1 showed the highest H$_2$ production rate of 46.6 μmol h^{-1} [64].
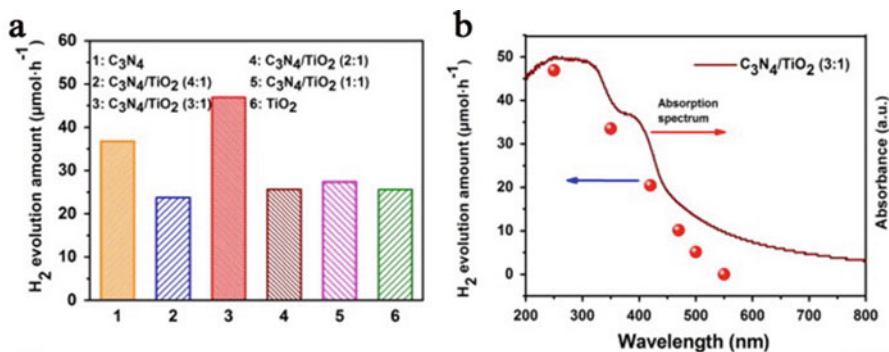
Fig. 7.17 (**a**) Photocatalytic H$_2$ evolution rates of the pure TiO$_2$ NBs, g-C$_3$N$_4$, and g-C$_3$N$_4$/TiO$_2$ NB heterostructure with different mass ratios; (**b**) wavelength dependence of H$_2$ evolution rate for g-C$_3$N$_4$/TiO$_2$ NBs (3:1) [64]. (Reprinted with permission from Ref. [64]. Copyright 2014, Elsevier)

7.3.3 Other Applications

Apart from the above applications, other applications of the g-C$_3$N$_4$/TiO$_2$ heterojunction catalysts have also been explored, such as the photocatalytic reduction of CO$_2$, treating heavy metal ion, as well as the inactivation of bacteria.

Guiyuan Jiang et al. fabricated a series of composites of g-C$_3$N$_4$ and in situ N-doped TiO$_2$ and then applied them to photocatalytic reduction of CO$_2$ under simulated light irradiation with water vapor at room temperature. Their research results showed efficient photocatalytic conversion of CO$_2$ to CO, and CH$_4$ was achieved. In addition, the photocatalytic activity and product selectivity were easy to adjust through simply varying the ratios of the precursor for g-C$_3$N$_4$ to the precursor for TiO$_2$ during the synthesis process of the catalyst. Moreover, as shown in Fig. 7.18, compared with g-C$_3$N$_4$ and commercial P25, the as-prepared g-C$_3$N$_4$-N-TiO$_2$ heterojunction photocatalysts showed improved photocatalytic performance for the reduction of CO$_2$, indicating the g-C$_3$N$_4$/TiO$_2$ heterojunction catalysts have good application prospects for mitigating the greenhouse effect and producing hydrocarbon and chemical compounds [65].

Guangshe Li et al. synthesized br-TiO$_2$/g-C$_3$N$_4$ by a facile calcination in air of brookite TiO$_2$ (br-TiO$_2$) hybridized with g-C$_3$N$_4$. The obtained samples were used for oxidation of toxic As^{3+} [42]. The intimately contacted hybrid br-TiO$_2$/g-C$_3$N$_4$ showed excellent photocatalytic activity in oxidation of As^{3+} to As^{5+}, which is less harmful than As^{3+}. Figure 7.19 indicated that the br-TiO$_2$/g-C$_3$N$_4$ catalyst with 35% weight ratio of the g-C$_3$N$_4$ exhibited much higher efficiency than pure br-TiO$_2$ and g-C$_3$N$_4$ for the application of As^{3+} oxidization.

Additionally, Taicheng An et al. investigated effective removal of biohazards from water using g-C$_3$N$_4$/TiO$_2$ hybrid photocatalyst [66]. The photocatalyst they synthesized was composed of micron-sized TiO$_2$ spheres wrapped with lamellar g-C$_3$N$_4$. A significantly improved visible light absorption and effectively reduced recombination of photo-generated electron–hole pairs were achieved by the
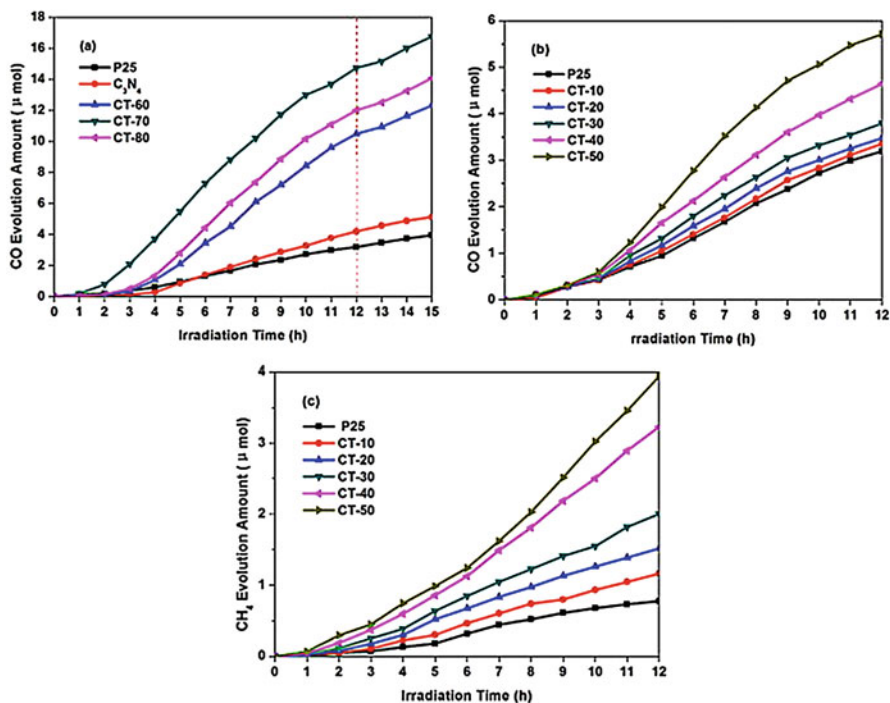
Fig. 7.18 (**a**) CO generation using different samples as a function of UV–vis light irradiation time. (**b**) CO generation using different samples as a function of UV–vis light irradiation time. (**c**) CH$_4$ generation using different samples as a function of UV–vis light irradiation time [65]. (Reprinted with permission from Ref. [65]. Copyright 2014, Elsevier)

combination of these two components. Using this hybrid photocatalyst, 107 cfu mL^{-1} of *Escherichia coli* K-12 could be completely inactivated within 180 min under visible light irradiation. Figure 7.20 showed that bacterial cells were seriously damaged during the photocatalytic inactivation processes, resulting in a severe leakage of intracellular components. Their research revealed that, through this kind of g-C$_3$N$_4$/TiO$_2$ heterojunction catalyst, bacterial cell destruction and water disinfection could be achieved easily. Besides, their results showed that substantial interaction between TiO$_2$ and g-C$_3$N$_4$ in the hybrid photocatalyst was a vital prerequisite for the enhancement of photocatalytic activity, which subsequently increased the trapping of the photoinduced charge carriers, benefiting for the production of reactive species. Furthermore, besides h$^+$, other reactive species such as subsequently generated ·O$_2^-$ and H$_2$O$_2$ also attacked biohazards, causing efficient photocatalytic inactivation and completely decomposition of bacteria.
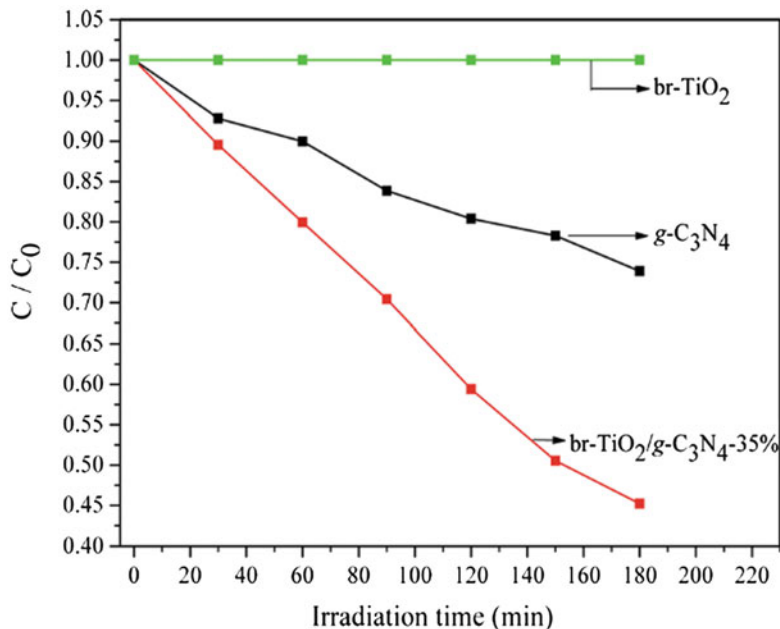
Fig. 7.19 Oxidation efficiency of As^{3+} over the hybrid br-TiO$_2$/g-C$_3$N$_4$–35%, pure g-C$_3$N$_4$, and 100% br-TiO$_2$ under visible light irradiation [42]. (Reprinted with permission from Ref. [42]. Copyright 2014, Royal Society of Chemistry)

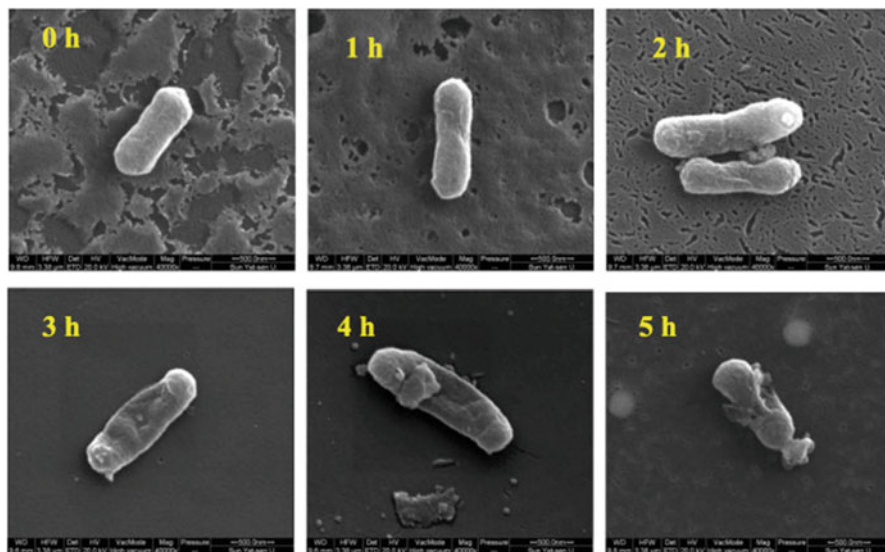**Fig. 7.20** SEM images of *E. coli* K-12 after the treatment of g-C$_3$N$_4$/TiO$_2$ hybrid photocatalysts at different times under visible light irradiation [66]. (Reprinted with permission from Ref. [66]. Copyright 2015, Elsevier)

7.4   Conclusions

This chapter summarized the recent progress of the research on the preparation methods and catalytic applications of g-C_3N_4/TiO_2 heterojunction catalysts. The synthesis methods of g-C_3N_4/TiO_2 heterojunction catalysts can be simply divided into three classes according to the order of each component prepared in the preparation process, which includes physically mixing g-C_3N_4 and TiO_2, growing TiO_2 on g-C_3N_4, and loading g-C_3N_4 on TiO_2. In spite of the different advantages and disadvantages exciting in the three different methods, every one of them can effectively form the heterojunctions between g-C_3N_4 and TiO_2, resulting in enhanced photocatalytic activity of the catalysts. The g-C_3N_4/TiO_2 heterojunction catalysts with excellent photocatalytic performance have been mainly applied in the photocatalytic degradation of organic pollutants, photolysis of water for producing H_2, photocatalytic reduction of CO_2, as well as the treatment of heavy metal ion and inactivation of bacteria.

Apart from the above research, g-C_3N_4/TiO_2 heterojunction catalysts are still worthy of exploration. Some groups found that there exists the phenomenon that the electron can transfer from dye to TiO_2, which implies that dye self-sensitized degradation also exists in this kind of composite system during the degradation process, providing the possibility for g-C_3N_4/TiO_2 heterojunction catalysts being applied to the dye-sensitized solar cells (DSSC). Moreover, some researchers have tried to design the ternary heterojunction catalysts such as g-C_3N_4/Ag/TiO_2 [41]. The studies on the structure design, the morphology control, and the expansion of applications related to g-C_3N_4/TiO_2 heterojunction catalysts are still significant. The heterojunction catalysts contain multiple components; therefore the stability of the heterojunction is not so satisfactory, and the interaction force between different components is still unknown. The preparation method of heterojunction catalysts looks more complex than the synthesis of other catalyst, and it still remains a great challenge for the development of a simplified synthesis method of the heterojunction catalysts.

References

1. Yang L, Wang L, Xing M et al (2016) Silica nanocrystal/graphene composite with improved photoelectric and photocatalytic performance. Appl Catal B Environ 180:106–112
2. Cheng C, Tan X, Lu D et al (2015) Carbon-dot-sensitized, nitrogen-doped TiO_2 in mesoporous silica for water decontamination through nonhydrophobic enrichment–degradation mode. Chem Eur J 21(49):17944–17950
3. Cheng C, Lu D, Shen B et al (2016) Mesoporous silica-based carbon dot/TiO_2 photocatalyst for efficient organic pollutant degradation. Microporous Mesoporous Mater 226:79–87
4. Liu F, Yu J, Tu G et al (2017) Carbon nitride coupled Ti-SBA15 catalyst for visible-light-driven photocatalytic reduction of Cr (VI) and the synergistic oxidation of phenol. Appl Catal B Environ 201:1–11

5. Yu J, Wang S, Low J et al (2013) Enhanced photocatalytic performance of direct Z-scheme g-C$_3$N$_4$–TiO$_2$ photocatalysts for the decomposition of formaldehyde in air. Phys Chem Chem Phys 15(39):16883–16890

6. Xing M, Shen F, Qiu B et al (2014) Highly-dispersed boron-doped graphene nanosheets loaded with TiO$_2$ nanoparticles for enhancing CO$_2$ photoreduction. Sci Rep 4:6341

7. Ansari MB, Min BH, Mo YH et al (2011) CO$_2$ activation and promotional effect in the oxidation of cyclic olefins over mesoporous carbon nitrides. Green Chem 13(6):1416–1421

8. Dong C, Xing M, Zhang J (2016) Economic hydrophobicity triggering of CO$_2$ photoreduction for selective CH$_4$ generation on noble-metal-free TiO$_2$–SiO$_2$. J Phys Chem Lett 7(15):2962

9. Xing M, Zhang J, Chen F et al (2011) An economic method to prepare vacuum activated photocatalysts with high photo-activities and photosensitivities. Chem Commun 47:4947

10. Dong C, Song H, Zhou Y et al (2016) Sulfur nanoparticles in situ growth on TiO$_2$ mesoporous single crystals with enhanced solar light photocatalytic performance. RSC Adv 6 (81):77863–77869

11. Qiu B, Xing M, Yi Q, Zhang J (2015) Angew Chem 127(36):10667

12. Ashkarran AA, Ghavamipour M, Hamidinezhad H et al (2015) Enhanced visible light-induced hydrophilicity in sol–gel-derived ag–TiO$_2$ hybrid nanolayers. Res Chem Intermed 41 (10):7299–7311

13. An L, Wang G, Cheng Y et al (2015) Ultrasonic-assisted synthesis of visible-light-driven TiO2/ Bi2O3 nanocomposite photocatalysts: characterization, properties and azo dye removal application. Res Chem Intermed 41(10):7449

14. Qiu B, Xing M, Zhang J (2014) Mesoporous TiO$_2$ nanocrystals grown in situ on graphene aerogels for high photocatalysis and lithium-ion batteries. J Am Chem Soc 136(16):5852–5855

15. Kitano S, Murakami N, Ohno T et al (2013) Bifunctionality of Rh^{3+} modifier on TiO$_2$ and working mechanism of Rh^{3+}/TiO$_2$ photocatalyst under irradiation of visible light. J Phys Chem C 117(21):11008–11016

16. Shiraishi Y, Takeda Y, Sugano Y et al (2011) Highly efficient photocatalytic dehalogenation of organic halides on TiO$_2$ loaded with bimetallic Pd–Pt alloy nanoparticles. Chem Commun 47 (27):7863–7865

17. Tsukamoto D, Shiro A, Shiraishi Y et al (2012) Photocatalytic H$_2$O$_2$ production from ethanol/ O$_2$ system using TiO$_2$ loaded with au–ag bimetallic alloy nanoparticles. ACS Catal 2 (4):599–603

18. Qi D, Xing M, Zhang J (2014) Hydrophobic carbon-doped TiO$_2$/MCF-F composite as a high performance photocatalyst. J Phys Chem C 118(14):7329–7336

19. Xie Y, Kum J, Zhao X et al (2011) Enhanced photocatalytic activity of mesoporous SN-codoped TiO$_2$ loaded with ag nanoparticles. Semicond Sci Technol 26(8):085–037

20. Wang P, Lei J, Xing M et al (2015) J Environ Chem Eng 3(2):961

21. Li H, Shen X, Liu Y, Wang L, Lei J, Zhang J (2016) J Alloys Compd 687

22. Ünlü H, Horing NJ, Dabowski J (eds) (2015) Low-dimensional and nanostructured materials and devices: properties, synthesis, characterization, modelling and applications. Springer

23. Li H, Shen X, Liu Y et al (2015) Facile phase control for hydrothermal synthesis of anatase-rutile TiO$_2$ with enhanced photocatalytic activity. J Alloys Compd 646:380–386

24. Zhang D, Gu X, Jing F et al (2015) High performance ultraviolet detector based on TiO$_2$/ZnO heterojunction. J Alloys Compd 618:551–554

25. Lin L, Yang Y, Men L et al (2013) A highly efficient TiO$_2$@ZnO n–p–n heterojunction nanorod photocatalyst. Nanoscale 5(2):588–593

26. Malik R, Tomer VK, Chaudhary V et al (2016) Facile synthesis of hybridized mesoporous au@TiO$_2$/SnO$_2$ as efficient photocatalyst and selective VOC sensor. ChemistrySelect 1 (12):3247–3258

27. Zhang ZL, Wang ML, Mao YL (2015) Mater Technol 30(1):2

28. Lu X, Wang Q, Cui D (2010) Preparation and photocatalytic properties of g-C$_3$N$_4$/TiO$_2$ hybrid composite. J Mater Sci Technol 26(10):925–930

29. Yang N, Li G, Wang W et al (2011) Photophysical and enhanced daylight photocatalytic properties of N-doped $TiO_2/g-C_3N_4$ composites. J Phys Chem Solids 72(11):1319–1324
30. Chai B, Peng T, Mao J et al (2012) Graphitic carbon nitride ($g-C_3N_4$)–Pt-TiO_2 nanocomposite as an efficient photocatalyst for hydrogen production under visible light irradiation. Phys Chem Chem Phys 14(48):16745–16752
31. Fu M, Pi J, Dong F et al (2013) A cost-effective solid-state approach to synthesize $g-C_3N_4$ coated TiO_2 nanocomposites with enhanced visible light photocatalytic activity. Int J Photoenergy 2013
32. Zhang J, Zhang M, Sun RQ et al (2012) A facile band alignment of polymeric carbon nitride semiconductors to construct isotype heterojunctions. Angew Chem 124(40):10292–10296
33. Dong F, Wu L, Sun Y et al (2011) Efficient synthesis of polymeric $g-C_3N_4$ layered materials as novel efficient visible light driven photocatalysts. J Mater Chem 21(39):15171–15174
34. Dong F, Sun Y, Wu L et al (2012) Facile transformation of low cost thiourea into nitrogen-rich graphitic carbon nitride nanocatalyst with high visible light photocatalytic performance. Cat Sci Technol 2(7):1332–1335
35. Chu VB, Cho JW, Park SJ et al (2014) Use of a precursor solution to fill the gaps between indium tin oxide nanorods, for preparation of three-dimensional $CuInGaS_2$ thin-film solar cells. Res Chem Intermed 40(1):49–56
36. Chen J, Qin S, Liu Y et al (2014) Preparation of a visible light-driven $Bi_2O_3–TiO_2$ composite photocatalyst by an ethylene glycol-assisted sol–gel method, and its photocatalytic properties. Res Chem Intermed 40(2):637–648
37. Yan H, Yang H (2011) $TiO_2-g-C_3N_4$ composite materials for photocatalytic H_2 evolution under visible light irradiation. J Alloys Compd 509(4):26–29
38. Zhou J, Zhang M, Zhu Y (2015) Photocatalytic enhancement of hybrid C_3N_4/TiO_2 prepared via ball milling method. Phys Chem Chem Phys 17(5):3647–3652
39. Gu L, Wang J, Zou Z et al (2014) Graphitic-C_3N_4-hybridized TiO_2 nanosheets with reactive {001} facets to enhance the UV-and visible-light photocatalytic activity. J Hazard Mater 268:216–223
40. Zhang L, Jing D, She X et al (2014) Heterojunctions in $g-C_3N_4/TiO_2$ (B) nanofibres with exposed (001) plane and enhanced visible-light photoactivity. J Mater Chem A 2(7):2071–2078
41. Chen Y, Huang W, He D et al (2014) Construction of heterostructured $g-C_3N_4/ag/TiO_2$ microspheres with enhanced photocatalysis performance under visible-light irradiation. ACS Appl Mater Interfaces 6(16):14405–14414
42. Zang Y, Li L, Xu Y et al (2014) Hybridization of brookite TiO_2 with $g-C_3N_4$: a visible-light-driven photocatalyst for As^{3+} oxidation, MO degradation and water splitting for hydrogen evolution. J Mater Chem A 2(38):15774–15780
43. Zhao S, Chen S, Yu H et al (2012) G-C_3N_4/TiO_2 hybrid photocatalyst with wide absorption wavelength range and effective photogenerated charge separation. Sep Purif Technol 99:50–54
44. Shen J, Yang H, Shen Q et al (2014) Template-free preparation and properties of mesoporous $g-C_3N_4/TiO_2$ nanocomposite photocatalyst. CrystEngComm 16(10):1868–1872
45. Li X, Liu P, Mao Y et al (2015) Preparation of homogeneous nitrogen-doped mesoporous TiO_2 spheres with enhanced visible-light photocatalysis. Appl Catal B Environ 164:352–359
46. Wang X, Yang W, Li F et al (2013) In situ microwave-assisted synthesis of porous N-$TiO_2/g-C_3N_4$ heterojunctions with enhanced visible-light photocatalytic properties. Ind Eng Chem Res 52(48):17140
47. Han C, Wang Y, Lei Y et al (2015) In situ synthesis of graphitic-C_3N_4 nanosheet hybridized N-doped TiO_2 nanofibers for efficient photocatalytic H_2 production and degradation. Nano Res 8(4):1199–1209
48. Sun Q, Lv K, Zhang Z et al (2015) Effect of contact interface between TiO_2 and $g-C_3N_4$ on the photoreactivity of $g-C_3N_4/TiO_2$ photocatalyst:(001) vs (101) facets of TiO_2. Appl Catal B Environ 164:420–427
49. Li H, Zhou L, Wang L (2015) In situ growth of TiO_2 nanocrystals on $g-C_3N_4$ for enhanced photocatalytic performance. Phys Chem Chem Phys 17(26):17406–17412

50. Li Y, Wang J, Yang Y et al (2015) Seed-induced growing various TiO$_2$ nanostructures on g-C$_3$N$_4$ nanosheets with much enhanced photocatalytic activity under visible light. J Hazard Mater 292:79–89
51. Wang J, Zhang WD (2012) Modification of TiO$_2$ nanorod arrays by graphite-like C$_3$N$_4$ with high visible light photoelectrochemical activity. Electrochim Acta 71:10–16
52. Fu M, Liao J, Dong F et al (2014) Growth of g-C$_3$N$_4$ layer on commercial TiO$_2$ for enhanced visible light photocatalytic activity. J Nanomater 2014:1
53. Boonprakob N, Wetchakun N, Phanichphant S et al (2014) Enhanced visible-light photocatalytic activity of g-C$_3$N$_4$/TiO$_2$ films. J Colloid Interface Sci 417:402–409
54. Zhu H, Chen D, Yue D et al (2014) In-situ synthesis of g-C$_3$N$_4$-P25 TiO$_2$ composite with enhanced visible light photoactivity. J Nanopart Res 16(10):2632
55. Lei J, Chen Y, Shen F et al (2015) Surface modification of TiO$_2$ with g-C$_3$N$_4$ for enhanced UV and visible photocatalytic activity. J Alloys Compd 631:328–334
56. Lei J, Chen Y, Wang L et al (2015) Surface modification of TiO$_2$ with g-C$_3$N$_4$ for enhanced UV and visible photocatalytic activity. J Mater Sci 50(9):3467
57. Zou XX, Li GD, Wang YN et al (2011) Direct conversion of urea into graphitic carbon nitride over mesoporous TiO$_2$ spheres under mild condition. Chem Commun 47(3):1066–1068
58. Zhou X, Jin B, Li L et al (2012) A carbon nitride/TiO$_2$ nanotube array heterojunction visible-light photocatalyst: synthesis, characterization, and photoelectrochemical properties. J Mater Chem 22(34):17900–17905
59. Li K, Gao S, Wang Q et al (2015) In-situ-reduced synthesis of Ti^{3+} self-doped TiO$_2$/g-C$_3$N$_4$ heterojunctions with high photocatalytic performance under LED light irradiation. ACS Appl Mater Interfaces 7(17):9023–9030
60. Ma J, Tan X, Yu T et al (2016) Fabrication of g-C$_3$N$_4$/TiO$_2$ hierarchical spheres with reactive {001} TiO$_2$ crystal facets and its visible-light photocatalytic activity. Int J Hydrog Energy 41 (6):3877–3887
61. Wei X, Shao C, Li X et al (2016) Facile in situ synthesis of plasmonic nanoparticles-decorated g-C$_3$N$_4$/TiO$_2$ heterojunction nanofibers and comparison study of their photosynergistic effects for efficient photocatalytic H$_2$ evolution. Nanoscale 8(21):11034–11043
62. Chen L, Zhou X, Jin B et al (2016) Heterojunctions in g-C$_3$N$_4$/B-TiO$_2$ nanosheets with exposed {001} plane and enhanced visible-light photocatalytic activities. Int J Hydrog Energy 41 (18):7292–7300
63. Gao ZD, Qu YF, Zhou X et al (2016) Pt-decorated g-C$_3$N$_4$/TiO$_2$ nanotube arrays with enhanced visible-light photocatalytic activity for H$_2$ evolution. ChemistryOpen 5(3):197–200
64. Zhong X, Jin M, Dong H et al (2014) TiO$_2$ nanobelts with a uniform coating of g-C$_3$N$_4$ as a highly effective heterostructure for enhanced photocatalytic activities. J Solid State Chem 220:54
65. Zhou S, Liu Y, Li J et al (2014) Facile in situ synthesis of graphitic carbon nitride (g-C$_3$N$_4$)-N-TiO$_2$ heterojunction as an efficient photocatalyst for the selective photoreduction of CO$_2$ to CO. Appl Catal B Environ 158:20–29
66. Li G, Nie X, Chen J et al (2015) Enhanced visible-light-driven photocatalytic inactivation of Escherichia coli using g-C$_3$N$_4$/TiO$_2$ hybrid photocatalyst synthesized using a hydrothermal-calcination approach. Water Res 86:17–24